Asymmetric Eruptive Filaments

Rui Liu[1], David Alexander, and Holly R. Gilbert[2]

Department of Physics and Astronomy, Rice University, Houston, TX 77005; rliu@rice.edu

ABSTRACT

Filaments are often observed to erupt asymmetrically, during which one leg is fixed to the photosphere (referred to as the *anchored leg*) while the other undertakes most of the dynamic motions (referred to as the *active leg*) during the eruptive process. In this paper, we present observations of a group of asymmetric eruptive filaments, in which two types of eruptions are identified: *whipping-like*, where the active leg whips upward, and hard X-ray sources shift toward the end of the anchored leg; and *zipping-like*, where the visible end of the active leg moves along the neutral line like the unfastening of a zipper as the filament arch rises and expands. During a zipping-like eruption, hard X-ray sources shift away from where the eruption initiates toward where the visible end of the active leg eventually stops moving. Both types of asymmetric eruptions can be understood in terms of how the highly sheared filament channel field, traced by filament material, responds to an external asymmetric magnetic confinement, where force imbalance occurs in the neighborhood of the visible end of the active leg. The dynamic motions of the active leg have a distinct impact on how hard X-ray sources shift, as observed by *RHESSI*.

Subject headings: Sun: filaments—Sun: CMEs—Sun: flares

1. Introduction

Solar filaments are relatively cool (5000–8000 K) and dense (10^{10}–10^{11} cm^{-3}) plasmas suspended in the hot (10^6 K) and tenuous (10^9 cm^{-3}) corona. Filaments only form in filament channels where all the chromospheric fibrils run parallel to the magnetic polarity boundary, representing the condition of maximum magnetic shear (e.g. Gaizauskas et al. 1997; Martin

[1]Current address: Center for Solar-Terrestrial Research, NJIT, Newark, NJ 07102

[2]Current address: NASA Goddard Space Flight Center, Greenbelt MD 20771

1998; Wang & Muglach 2007). A helical flux rope configuration is often invoked in the modeling of filaments, with its lower portion naturally able to support the filament mass in, and thermally isolate it from, the surrounding corona (e.g., Low 1996). Models adopting sheared arcade geometries (e.g., Antiochos & Klimchuk 1991) or thermodynamic variability (e.g., Karpen et al. 2001) can also explain the presence of chromospheric material in the corona. The existence of a flux rope after the onset of the eruption is, however, widely accepted, thanks in part to in-situ observations of interplanetary magnetic clouds (see the review by Burlaga 1991).

The dynamic evolution of eruptive filaments is observed to take different forms, including *loop-like*, where a single coherent loop-shape structure erupts (e.g. Gopalswamy & Hanaoka 1998); *kinking*, where the filament twists from the loop-shape to an inverse γ-shape, and then into a 'knot' with two filament legs crossing each other (e.g. Alexander et al. 2006); and *asymmetric*, where the filament eruption starts at one end while the other end remains fixed to the photosphere (e.g. Tripathi et al. 2006). Tripathi et al. (2006) studied the EUV brightening that occurred during filament eruptions observed by *SOHO* EIT and found that when the filament erupted asymmetrically the EUV brightening propagated from the end point where the eruption started towards the anchored end point. In contrast, when the filament erupted symmetrically, the propagation of the EUV brightening started at the middle of the filament channel and propagated towards both end points. Tripathi et al. (2006) suggested that the propagation of the EUV brightening represents successive reconnections in a simple three-dimensional extension of the standard two-dimensional flare model. A similar interpretation has been proposed for the propagation of the soft X-ray loops in giant arcade formation events (Isobe et al. 2002).

The motions of hard X-ray (HXR) sources in the chromosphere are generally regarded as being directly related to the presumed magnetic reconnection in the corona. In the classic scenario (e.g., Priest & Forbes 2002), the two HXR footpoint sources move apart as successive field lines are reconnected at higher and higher altitude, with the X-point of the reconnection moving upward, which is often highlighted by a HXR coronal or looptop source (Tsuneta et al. 1992). Three types of motions of HXR footpoint sources have been identified by Bogachev et al. (2005) in a study of 31 flares observed by the Hard X-ray Telescope on board *Yohkoh*. In this study, 4 flares show motions away from and nearly perpendicular to the neutral line (Type I), in agreement with the standard flare model; 8 flares show antiparallel motions along the neutral line (Type II), indicating the relaxation of the sheared field; 11 flares show motions in the same direction along the neutral line (Type III), suggesting "a displacement of the particle acceleration region during a flare"; and the remaining 8 flares display a combination of the three basic types. This classification is supported by a more recent study using *RHESSI* data (Gan et al. 2008). A new type of

motion has also been revealed in *RHESSI* observations, namely, the converging motion of conjugate footpoints during the initial phase of flares (e.g., Ji et al. 2006). Grigis & Benz (2005) suggested that the Type III motion identified by Bogachev et al. (2005) could be produced by the asymmetric eruption of a filament, so that "the arcade erupts in a manner similar to the opening of a zipper", although no filament is observed in the event that they studied.

In this paper we investigate a group of asymmetric filament eruptions, all of which are associated with the Type III motion of HXR sources. Observations are presented in §2–4. and the interpretation of the observations in §5.

2. Observations and Data Analysis

2.1. Overview of Observations

As defined here, during an asymmetric filament eruption, the leg that is fixed to the photosphere is referred to as the *anchored leg*, and the leg that undertakes most of the observed dynamic motions is referred to as the *active leg*. Two types of asymmetric filament eruptions are identified in our study: *whipping-like*, where the active leg whips upward, occasionally extending into the *SOHO* LASCO field of view (FOV); and *zipping-like*, where the visible end of the active leg moves along the neutral line like the unfastening of a zipper. Details of two types of asymmetric eruptions are provided in the case studies below, where §3 is dedicated to whipping-like events, and §4 to zipping-like events. Table 1 lists the events we have studied. All the filaments studied here are *eruptive* (Gilbert et al. 2000), i.e., all or some of the filament material escapes the solar gravitational field, resulting in a coronal mass ejection (CME).

2.2. Co-Alignment

With the exception of the 2005 July 29 event, the other three events are observed by the *Transition Region and Coronal Explorer (TRACE)* spacecraft (Handy et al. 1999). The *TRACE* telescope has a field of view of 8.5 arcmin × 8.5 arcmin and a spatial resolution of 1 arcsec (0.5 arcsec pixels) with a typical time cadence of less than one minute. The determination of its absolute pointing is a little more complicated than is the case with a full disk imager where the solar limb provides a reference. Moreover, an unknown and time-varying offset is caused by flexures of the instrument metering tube that supports the telescope. This can result in errors of more than $10''$ in the *TRACE* pointing knowledge

(Fletcher & Hudson 2001). Thus, care must be taken in comparing *TRACE* observations with other instruments. It is also known that the *TRACE* EUV channel pointing is offset with respect to the *TRACE* WL (white-light) channel, due to the different focus positions of the two, which has been taken into account in processing the *TRACE* images.

The 2005 July 27 event is a limb event, thus the only method available for correcting the *TRACE* pointing is to cross-correlate the *TRACE* 171 Å images with nearly-simultaneous EIT 195 Å images (Gallagher et al. 2002), assuming the pointing information of the EIT full disk observations is correct. For the 2005 July 30 event, only *TRACE* 171 Å images are available, so we followed the same procedure as used for the 2005 July 27 event. For the 2003 Aug 25 event, *TRACE* 171 Å, 1600 Å (UV continuum), and WL images are all available. For this event, three different methods can be used to correct the *TRACE* pointing. By cross-correlating *TRACE* 171 Å and EIT 195 Å images, we found that the *TRACE* pointing should be offset by about 14″ in the X direction and about -2″ in the Y direction (left panel of Fig. 1). Following the method by Metcalf et al. (2003), we cross-correlated an image obtained in the *TRACE* WL channel and an MDI continuum image, using *trace_mdi_align* in the SolarSoftWare (SSW; Freeland & Handy 1998), and found that the *TRACE* pointing should be offset by 7″ in the X direction and -6″ in the Y direction. Finally, following Aulanier et al. (2000), we overlaid one *TRACE* 1600 Å image with the nearly simultaneous MDI line-of-sight magnetogram, manually adjusting the alignment between the facular brightening and the weak network fields (right panel of Fig. 1). The result is that *TRACE* 1600 Å should be offset by 14″ in the X direction and -4″ in the Y direction, approximately consistent with the co-alignment result using *TRACE* 171 Å and EIT 195 Å images, but there is a relatively large discrepancy when compared with the co-alignment result using the white-light image (about 7″ in the X direction). This is most likely caused by projection since the active region was close to the east limb. Thus, we adopt the co-alignment approach using the method of Gallagher et al. (2002) for the *TRACE* 171 Å images, and the approach using the method of Aulanier et al. (2000) for the *TRACE* 1600 Å images. Table 2 summarizes the *TRACE* pointing corrections conducted in this paper.

3. Whipping-like Events

We present two whipping-like asymmetric filament eruptions in this section. The eruption on 2003 August 25 was observed to originate from NOAA active region 10442 when it was located in the southeast quadrant of the solar disk, and the eruption on 2005 July 27 was observed to originate from NOAA active region 10792 when it was located on the east limb.

3.1. 2003 August 25 Event

In the 2003 August 25 event, the eastern leg of the filament is anchored in the neighborhood of the trailing sunspot that is of positive polarity, while its western leg in the neighborhood of the leading sunspot that is of negative polarity (left panel of Fig. 1). From 01:00–02:30 UT, the loop-shaped filament slowly rose and the filament arch gradually expanded, which we define as the activation phase of the eruption. The filament suddenly jumped upward at about 02:26 UT (Fig. 2*a*). By 02:39 UT (Fig. 2*c* and 2*f*), the western leg of the filament apparently disconnected from the solar surface, while the eastern leg was still anchored till 02:51 UT (Fig. 2*i* and 2*l*). After that, the eastern leg also faded, presumably due to mass depletion because of either material ejecting into higher corona or draining down to the solar surface.

During the activation phase, two bright dots appeared within each of the two opposite-polarity dark sunspots in *TRACE* 1600 Å images, and gradually brightened, which is not observed in other *TRACE* channels (WL or EUV). All the 1600 Å images used in our study, from 00:47 to 04:20 UT, have the same exposure time, ~ 0.86 s. The brightness (in DN/s) is measured by summing the pixel values over an 11 pixel $\times$ 11 pixel box enclosing each dot (Fig. 3*a*). From 02:20–02:30 UT, the bright dot in the trailing sunspot flashed, with the brightness increasing exponentially (Fig. 4*c*), coincident with the sudden jump of the filament (Fig. 4*a*). The brightness of the dot in the leading sunspot also increased, but much more slowly than the dot in the trailing sunspot (Fig. 4*c*). Both bright dots also expanded in size. Our measurement stops when the brightening in the trailing sunspot began to expand beyond the defined box at 02:27:26 UT. From 02:30 UT onward, both bright dots developed into ribbons extending across the sunspots, connecting with flare ribbons outside (Fig. 3*b*). Intriguingly, the filament leg whipped upward from the neighborhood of the leading sunspot, where the umbral brightening is weaker. The brightness profile of the bright dot within the trailing sunspot, on the other hand, is more closely correlated with the filament's displacement profile (Fig. 4*a* and 4*c*).

The eruption is associated with a *GOES* class C3.7 flare. As the eruption progressed, the HXR sources in the low energy range (6–12 keV; green contours), which show thermal footpoint emission, appeared at first in the neighborhood of the leading sunspot, then in the neighborhood of the both sunspots, and finally settled in the neighborhood of the trailing sunspot (Fig. 3*b*–*d*). The HXR sources in the higher energy bands (12–25 keV, blue contours; and 25–50 keV, purple contours) can only be spatially resolved in *RHESSI* data after 02:46 UT. They were located in the neighborhood of the trailing sunspot, co-spatial with the soft X-ray source (Fig. 3*d*–*f*). From 02:32:12 UT till 02:42:18 UT, the centroid of the 6–12 keV X-ray source shifted by about 33″, with an average 'equivalent' speed of about 40 km s^{-1}

during the course of the filament eruption.

The projected displacements of the filament are obtained by measuring the top of the filament along a fiducial as shown in Fig. 2*a*. The measurement represents a lower limit, as the fiducial mostly cut through the anchored leg, while the active leg had whipped out of the *TRACE* FOV. The measurement is also compromised by the large uncertainties that are introduced when the contrast of the filament rapidly decreases as the eruption progressed. Fig. 4*a* shows that the overall profile can be roughly fit with a power law function of the form, $h = a + bt + ct^m$, with $\chi^2_\nu = 9.90$[1], and $m = 3.6 \pm 0.06$. The result is very similar to that obtained by Alexander et al. (2002), who found that the best fit for the height-time profile of the early phase of a CME observed by the Soft X-Ray Telescope on board *Yohkoh* took the form $h_0 + v_0 t + ct^{3.7\pm0.03}$. The power law fit is slightly better than the exponential fit (e.g., Gallagher et al. 2003), $h = a + b\,exp(ct)$, with $\chi^2_\nu = 20.89$, a result in agreement with Schrijver et al. (2008), who found that in the two cases they studied the power law fit with $m \gtrapprox 3$ is superior to the exponential fit for the rapid-acceleration phase of the filament eruption. However, the power-law fit uses four parameters to fit the data compared to three parameters in the exponential fit.

The acceleration derived from the projected displacements by numerical differentiation shows that the acceleration peaked prior to the onset of the X-ray emission (Fig. 4*b*). The acceleration derived from the power law fit or exponential fit, however, can only be valid over a relatively short height range as the acceleration profile usually has a peak at some height in the low corona, followed by a decay (e.g., Gallagher et al. 2003). The timing between the peak acceleration of the filament and the onset of the flare suggests that the eruption may have been triggered by an ideal instability (see the discussion in §5.3), as indicated by the exponential increase of the UV brightness of the bright dot within the trailing sunspot prior to the flare, as well as the exponential increase of the filament's 'height'.

3.2. 2005 July 27 Event

Fig. 5 shows the eruptive filament on 2005 July 27, observed by the *TRACE* 171 Å filter (see the detailed multi-wavelength investigation by Chifor et al. 2006). The eruption is associated with a *GOES* class M3.7 flare starting at 04:00 UT. RHESSI data were unfortunately not available from 04:06 UT till 04:48 UT due to RHESSI night and an SAA (South Atlantic Anomaly) passage. Just before *RHESSI* night time, the reconstruction of a 12-25 keV HXR

[1] χ^2_ν is the standard deviation of the residuals, defined as χ^2/N, where χ^2 is the chi-square estimator and N is the number of the degrees of freedom.

source (red contours at 04:01 UT in Fig. 5) shows that the HXR sources are located where the filament eruption initiated. During the eruption, the filament spine extended upward above 0.46 $R_\odot$, beyond the field of view of *SOHO* EIT. The filament ultimately disappeared at about 05:02 UT in *TRACE* 171 Å data and 05:24 UT in EIT 195 Å data, with the mass presumably ejected outward into the higher corona. A filament thread located in the foreground, however, remained intact throughout the eruptive process (Fig. 5).

Fig. 6 shows the evolution of the coronal HXR source for the 2005 July 27 event, seen in the 12-25 (Fig. 6*a*) and 25-50 keV (Fig. 6*b*) energy ranges, respectively. From 04:51 to 05:28 UT, the centroid of the HXR source in the 12–25 keV energy range shifted by about 30″, with an average 'equivalent' speed of $\sim$ 10 km s^{-1}. From 04:52 to 04:59 UT, the centroid of the HXR source in the 25–50 keV energy range shifted by about 9″, with an average 'equivalent' speed of $\sim$ 16 km s^{-1}. Both shifts are projected in the northeast direction, deviating from the radial direction, but in a similar direction to that of the filament whipping.

4. Zipping-like Events

Two zipping-like asymmetric eruptions were observed on 2005 July 27 and July 30, respectively, both from NOAA active region 10792 (the whipping-like event on July 27 also originated from this active region). Fig. 7 shows the active region in Hα obtained at Big Bear Solar Observatory (BBSO) at 15:39:57 UT on 2005 August 3, overlaid with a *SOHO* MDI line-of-sight magnetogram obtained at 15:59:02 UT on 2005 August 3, when the active region was at disk center. The active region has an reverse S-shaped polarity boundary (also termed neutral line, or polarity inversion line), which separates regions of opposite-polarity, line-of-sight magnetic fields. The extended neutral line is essentially composed of three predominantly north-south oriented segments (referred to as eastern, central and western neutral lines in this paper), outlined by dark filaments.

4.1. 2005 July 29 Event

Fig. 8 shows the filament eruption on 2005 July 29, observed in the *SOHO* EIT 304 Å filter. At 17:36:10 UT, the western leg of the filament is anchored at the central neutral line, while the eastern leg seems to be anchored to the north of the eastern neutral line. As the filament erupted, its arch expanded, and rotated counter-clockwise, as the active, eastern leg moved southward, associated with a southward shifting of the HXR footpoint sources (Fig. 9). From 17:24:52 UT to 17:30:56 UT, the centroid of the 12–25 keV X-ray source

shifted by about 70″, with an average 'equivalent' speed of about 140 km s^{-1}. At 18:24:10 UT, the active leg appeared to settle to the south of the anchored leg. Most of the filament material, however, fell back to the solar surface, and the eruption only resulted in a small jet-like CME.

Fig. 10 shows the same eruption observed by the CHIP instrument (Elmore et al. 1998; MacQueen et al. 1998) operated at the Mauna Loa Solar Observatory (MLSO). At 17:36:09 UT (Fig. 10*a*), the western half of the filament arch was blue-shifted while the other half red-shifted, which is consistent with with the observed expansion of the east-west oriented filament on the east limb. In Fig. 10*b*–*c*, both red and blue shifts were observed simultaneously within the anchored, western leg, indicating the twisting motion of the filament spine, which suggests that the filament field may have a flux-rope configuration at this time. One possibility is that it is a manifestation of the 'untwisting' of the magnetic flux rope. This naturally occurs when the filament arch expands so that the length of the flux rope increases. The field line pitch, q, therefore decreases if the total twist of the flux rope, $Tw(q) = \Phi^2/2\pi \oint q\, dl$, where Φ is the magnetic flux through the flux-rope cross section, is reasonably assumed to be approximately constant, or at least not to increase during the eruptive process. In contrast, the eastern leg was still red-shift dominated at 17:51:07 UT (Fig. 10*d*), suggesting that the expansion occurs primarily due to the dynamic evolution of the active leg. As the expansion speed of the filament arch decreased, the mixed red and blue shifts appeared within both legs (Fig. 10*d*–*e*). The transition of the Doppler signals within the active leg, from red shift at 17:51:07 UT (Fig. 10*d*), to mixed red and blue shifts at 17:54:07 UT (Fig. 10*e*), and then to blue shift at 17:57:09 UT (Fig. 10*f*), can be naturally interpreted as due to the expansion of filament, followed by the counter-clockwise rotating motion of the filament arch, coupling to the counter-clockwise twisting motion within the filament spine itself.

4.2. 2005 July 30 Event

The 2005 July 30 event involves two asymmetric eruptions. The first eruption, occurring at about 05:10 UT, is a small whipping-like event, hereafter being referred to as F_1. The second eruption, occurring at about 06:00 UT, is a zipping-like event, hereafter being referred to as F_2, on which we will concentrate in this section. F_1 is primarily aligned along the southern half of the reverse S-shaped neutral line, with one end at the western neutral line, the other at the central neutral line. F_2 is primarily aligned along the northern half of the reverse S-shaped neutral line, with one end at the central neutral line, the other end at the eastern neutral line (Fig. 11*a*). Prior to the eruption of F_1, it can be seen that F_2

experienced some marked activity, evident as mass moving along the filament spine. At 04:08:54 UT (Fig. 11*b*), the visible end of F_2 at the central neutral line extended further south to the close neighborhood of the end of F_1 at the central neutral line, indicated by a white arrow.

The whipping-like eruption of F_1 was associated with a *GOES* class C9.4 flare starting from about 05:03 UT, coincident with an EUV brightening at the western end of F_1, indicated by a white arrow in Fig. 11*a*. An ejection was observed to originate from that EUV brightening, which activated F_1 (Fig. 11*b*). F_1 started to whip upward from its western end at 05:06:50 UT. The reconstructed HXR sources in the 12–25 keV energy band are also located at the western end of F_1 (Fig. 11*b*–*c*). At about 05:30 UT, the top of F_1 reached the eastern boundary of the *TRACE* FOV. Some material was ejected beyond the *TRACE* FOV, resulting in a small CME with an angular width of 30°. This CME was only visible in one LASCO C2 image at 05:57 UT (no detection in the C3 image at 06:40 UT). A halo-CME was observed in the next C2 image at 06:50 UT, then in the C3 image at 07:00 UT, which is obviously associated with the eruption of F_2 at about 06:30 UT (see below). Most of the filament material, however, fell back to the solar surface, toward the anchored end at the central neutral line (Fig. 11*d*).

The zipping-like eruption of F_2 was associated with a *GOES* class X1.3 flare starting from about 06:17 UT. Just prior to the eruption, the active leg appeared partly in emission in *TRACE* 171 Å (Fig. 12*a*–*b*). The activation of the filament appeared to start from further north of the central neutral line (Fig. 12*b*), but as the eruption progressed, the visible end of the active leg extended successively southward. The whole active leg took off at about 06:28 UT. The anchored leg can still be seen at 06:32:31 UT, but was significantly fainter partly due to the decreasing contrast as the post-flare arcade brightened. The eruption resulted in a halo CME.

Right after the active leg erupted, the 'harder' (> 25 keV) footpoint sources, a manifestation of electron-ion bremsstrahlung produced by energetic electrons accelerated at reconnection sites in the corona, shifted southward along the neutral line; the 'softer' (12–25 keV) source, primarily due to the chromospheric evaporation of heated chromospheric plasma (e.g., Antonucci et al. 1982), remained localized to the region surrounding the site where the eruption initiated, i.e., in the north of the central neutral line (Fig.12*d*–*e*). From 06:28:36 UT till 06:37:56 UT, the centroid of the HXR source in the 25–50 keV energy range shifted by about 38″, with an average 'equivalent' speed of about 50 km s^{-1}. During the same period of time, the centroid of the HXR source in the 50–100 keV energy range shifted by about 30″ with an average 'equivalent' speed of about 40 km s^{-1}. In the same direction of the HXR source shifting, the brightening of the EUV post-flare arcade propagated along the neutral

line (Fig. 13).

5. Interpretation of the Observations

5.1. Interpretation of Whipping-like Events

Fig. 14 summarizes our understanding of the whipping-like events. Ideologically, the whipping motion of the filament can be trigged by "tether release" (top panel of Fig. 14; also see the review by Klimchuk 2001). The field lines that provide the confinement for the filament (potential-like loops in Fig. 14) are usually termed *tethers*, analogous to the ground-anchored ropes that hold down a buoyant balloon. Tether-release may take place slowly, but systematically, at one end of the filament, and therefore the strain on the remaining tethers increases gradually to a critical point that the force balance between the upward magnetic pressure, $-\nabla B^2/8\pi$, of the highly sheared filament channel field and the downward tension, $(1/4\pi)(\mathbf{B}\cdot\nabla)\mathbf{B}$, of the overlying quasi-potential field is disrupted at that end, while the force balance still roughly maintains at the other end. The filament, therefore, whips upward in an explosive fashion from the end with the force imbalance. The whipping motion would stretch the overlying magnetic field lines with a current sheet forming underneath the filament, where field lines may reconnect (bottom panel of Fig. 14). The reconnection in turn enables the active leg to whip upward more, which results in a positive feedback for the whole eruptive process. As more and more field lines overlying the filament are stretched and reconnect successively, the HXR footpoint source would shift along the neutral line toward the end of the anchored leg of the filament, and the HXR coronal source would shift upward, at the same time toward the anchored end, as the cartoon implies. The mass in the active leg could either be depleted quickly due to mass draining, or fail to keep up with the whipping motion, and therefore the end of the active leg is observed to be apparently detached from the solar surface, to which the filament field may be still connected, as indicated by the dotted line in the bottom panel of Fig. 14.

5.2. Interpretation of Zipping-like Events

It is interesting that the two zipping-like eruptions 'mirror' each other (see Fig. 15): the filament on 2005 July 29 has one leg anchored at the central neutral line while the visible end of the other leg moved southward along the eastern neutral line, associated with the southward shifting of the HXR sources; the filament, F_2, on 2005 July 30, however, has one leg anchored at the eastern neutral line and the visible end of the other leg moving

southward along the central neutral line, also associated with the southward shifting of the HXR sources. Since the neutral line is curved, the filament arch rotated as part of the zipping process, which was detected by MLSO/CHIP instrument in the 2005 July 29 event.

The schematic diagrams in Fig. 15 are further simplified (in absence of the S-shaped polarity boundary) in Fig. 16 which summarizes our interpretation of zipping-like asymmetric filament eruptions. Prior to the eruption, the filament has an apparent symmetric loop-shape, represented by a thick solid line in Fig. 16. But the lower part of the active leg, lying very low and flat in the solar atmosphere, is actually anchored farther away. It is invisible because it is not loaded with mass, as indicated by a dotted line. The eruption is probably trigged by tether release in the neighborhood of the visible end of the active leg, as indicated by an x mark in the top panel of Fig. 16. The filament arch then rises and expands toward the invisible end of the active leg. The compact potential-like loops that overly the lower part of the active leg are stretched due to the expansion and rise of the filament arch, and thereby reconnect beneath the filament, which result in the shifting of HXR sources toward the invisible end of the active leg, away from where the eruption initiates. At the same time, filament material drains down along the filament leg, making more and more of the lower part of the active leg visible, and creating an impression that the 'footpoint' of the active leg moves along the neutral line as the eruption progresses.

5.3. Discussion and Conclusion

Both the whipping-like and zipping-like asymmetric filament eruptions can be understood in terms of how the highly sheared filament channel field, traced by the filament material, responds to an external asymmetric magnetic confinement. This asymmetric confinement may manifest as a force imbalance due to tether release occurring in the neighborhood of the visible end of the active leg, as illustrated in Fig. 14 and Fig. 16. The asymmetric eruption can also, presumably, be triggered by certain ideal instabilities, e.g., the torus instability (Kliem & Török 2006; Török & Kliem 2007; Fan & Gibson 2007). If the overlying field at one end of the filament declines more rapidly with height than at the other end, the eruption would, as a consequence, be asymmetric, as the more sharply decreasing field is more susceptible to the torus instability. Recently, Schrijver et al. (2008) showed numerical simulations of the torus instability that approximate the height evolution of the whipping-like filament in the 2005 July 27 event. During its rapid-acceleration phase, the height-time profile is best characterized by $h(t) \propto t^m$ with $m \gtrapprox 3$. They noted that such an evolution is incompatible with so far published height-time profiles of breakout, MHD-instability, or catastrophe models. Schrijver et al. (2008), however, also acknowledged that reconnection

occurred even before the rapid-acceleration phase in the 2005 July 27 event, as suggested by the observed precursor soft and hard X-ray emission, and that the torus instability model is highly sensitive to the initial as well as the boundary conditions, which can yield a range of different hight-time profiles. Thus, the rise profile of the filament alone is far from sufficient to determine the destabilizing/driving process, especially when multiple processes could take place in the same event (e.g., Liu et al. 2008).

During the asymmetric filament eruption, the active leg can either whip upward, if it is anchored at the location where the eruption initiates; or 'zip' away from the visible end of the active leg, where the eruption initiates, toward the 'invisible' end of the active leg. The 'invisible' end later becomes visible during the zipping process with mass draining down along the field line, as illustrated in Fig. 16. This temporary 'invisibility' of the field line that connects the visible end of the active leg to its real anchor point on the solar surface is due to the lack of the filament mass, which may have been depleted via mass-draining.

In the case of whipping-like eruptions, HXR sources shift toward the anchored end of the filament along the neutral line; in zipping-like eruptions, HXR sources shift away from where the eruption initiates toward the 'invisible' end of the active leg. The shifting of HXR sources is caused by overlying field lines successively stretched and thereby reconnected due to the whipping or zipping motions of the active leg. However, for small events, the whipping or zipping motions of the filament may not be able to stretch the overlying field lines to the extent that they form a current sheet and reconnect, which may be the case in the small whipping-like event on 2005 July 30. In conclusion, the asymmetric dynamic motion of the active leg has a distinct impact on the reconnection site of the overlying field in the corona, and thereby the shifting of HXR sources. In general, the reconnection site in the corona should be affected in a similar fashion by the asymmetric eruption of a magnetic flux rope whether it is loaded with filament mass or not. The mechanisms leading to asymmetric eruptions, however, remains uncertain and requires further investigation.

The authors are grateful to the *TRACE, RHESSI, SOHO,* MLSO and BBSO instrument teams for the excellent data. This work was supported by SHINE under NSF grant ATM-0353345.

REFERENCES

Alexander, D., Liu, R., & Gilbert, H. R. 2006, Astrophys. J., 653, 719

Alexander, D., Metcalf, T. R., & Nitta, N. V. 2002, Geophys. Res. Lett., 29, 41

Antiochos, S. K. & Klimchuk, J. A. 1991, Astrophys. J., 378, 372

Antonucci, E., Gabriel, A. H., Acton, L. W., Leibacher, J. W., Culhane, J. L., Rapley, C. G., Doyle, J. G., Machado, M. E., & Orwig, L. E. 1982, Sol. Phys., 78, 107

Aulanier, G., DeLuca, E. E., Antiochos, S. K., McMullen, R. A., & Golub, L. 2000, Astrophys. J., 540, 1126

Bogachev, S. A., Somov, B. V., Kosugi, T., & Sakao, T. 2005, Astrophys. J., 630, 561

Burlaga, L. F. 1991, in Physics of the Inner Heliosphere, ed. E. Schwenn, R. & Marsch, Vol. 2 (Springer-Verlag), 1–22

Chifor, C., Mason, H. E., Tripathi, D., et al. 2006, Astron. Astrophys., 458, 965

Elmore, D. F., Card, G. L., Chambellan, C. W., et al. 1998, Appl. Opt., 37, 4270

Fan, Y. & Gibson, S. E. 2007, Astrophys. J., 668, 1232

Fletcher, L. & Hudson, H. 2001, Sol. Phys., 204, 69

Freeland, S. L. & Handy, B. N. 1998, Sol. Phys., 182, 497

Gaizauskas, V., Zirker, J. B., Sweetland, C., & Kovacs, A. 1997, Astrophys. J., 479, 448

Gallagher, P. T., Dennis, B. R., Krucker, S., et al. 2002, Sol. Phys., 210, 341

Gallagher, P. T., Lawrence, G. R., & Dennis, B. R. 2003, Astrophys. J. Lett., 588, L53

Gan, W. Q., Li, Y. P., & Miroshnichenko, L. I. 2008, Adv. Space Res., 41, 908

Gilbert, H. R., Holzer, T. E., Burkepile, J. T., & Hundhausen, A. J. 2000, Astrophys. J., 537, 503

Gopalswamy, N. & Hanaoka, Y. 1998, Astrophys. J. Lett., 498, L179

Grigis, P. C. & Benz, A. O. 2005, Astrophys. J., 625, L143

Handy, B. N., Acton, L. W., Kankelborg, C. C., et al. 1999, Sol. Phys., 187, 229

Isobe, H., Shibata, K., & Machida, S. 2002, Geophys. Res. Lett., 29, 10

Ji, H., Huang, G., Wang, H., Zhou, T., Li, Y., Zhang, Y., & Song, M. 2006, Astrophys. J. Lett., 636, L173

Karpen, J. T., Antiochos, S. K., Hohensee, M., Klimchuk, J. A., & MacNeice, P. J. 2001, Astrophys. J. Lett., 553, L85

Kliem, B. & Török, T. 2006, Phys. Rev. Lett., 96, 255002

Klimchuk, J. A. 2001, in Space Weather (Geophysical Monograph 125), ed. P. Song, H. Singer, & G. Siscoe (Washington: American Geophysical Union), 143

Liu, R., Gilbert, Holly, R., Alexander, D., & Su, Y. 2008, Astrophys. J., 680, 1508

Low, B. C. 1996, Sol. Phys., 167, 217

MacQueen, R. M., Blankner, J. G., Elmore, D. F., et al. 1998, Sol. Phys., 182, 97

Martin, S. F. 1998, Sol. Phys., 182, 107

Metcalf, T. R., Alexander, D., Hudson, H. S., & Longcope, D. W. 2003, Astrophys. J., 595, 483

Priest, E. R. & Forbes, T. G. 2002, Astro. Astrophys. Rev., 10, 313

Schrijver, C. J., Elmore, C., Kliem, B., et al. 2008, Astrophys. J., 674, 586

Török, T. & Kliem, B. 2007, Astron. Nachr., 328, 743

Tripathi, D., Isobe, H., & Mason, H. E. 2006, Astron. Astrophys., 453, 1111

Tsuneta, S., Hara, H., Shimizu, T., Acton, L. W., Strong, K. T., Hudson, H. S., & Ogawara, Y. 1992, Publ. Aston. Soc. Jpn., 44, L63

Wang, Y.-M. & Muglach, K. 2007, Astrophys. J., 666, 1284

Table 1: List of events studied in this paper

Date	Time[1] (UT)	Type[2]	CME[3] (deg)
2003 August 25	02:30	Whipping	61
2005 July 27	05:00	Whipping	360
2005 July 29	18:00	Zipping	15
2005 July 30	03:00	Whipping	30
	05:00	Zipping	360

[1]The approximate time when the filament erupted

[2]The types of the asymmetric eruption

[3]The angular width of the CME associated with the asymmetric filament eruption, adopted from the *SOHO* LASCO CME catalog.

Table 2: *TRACE* pointing correction

	X_{off} (arcsec)	Y_{off} (arcsec)	Method
2003 Aug 25	7.3	-6.0	Metcalf et al. (2003)
	13.9 ± 1.74	-1.6 ± 1.33	Gallagher et al. (2002)[1]
	14	-4	Aulanier et al. (2000)
2005 July 27	2.2 ± 0.42	-17.9 ± 0.74	Gallagher et al. (2002)
2005 July 30	4.2 ± 0.68	-14.8 ± 0.68	Gallagher et al. (2002)

[1]When multiple EIT 195 Å images are used to correct the *TRACE* pointing, the *TRACE* offset is written in the form of $\overline{X_{off}} \pm \sigma$ and $\overline{Y_{off}} \pm \sigma$, where the barred variable indicates the average and σ is the standard deviation.

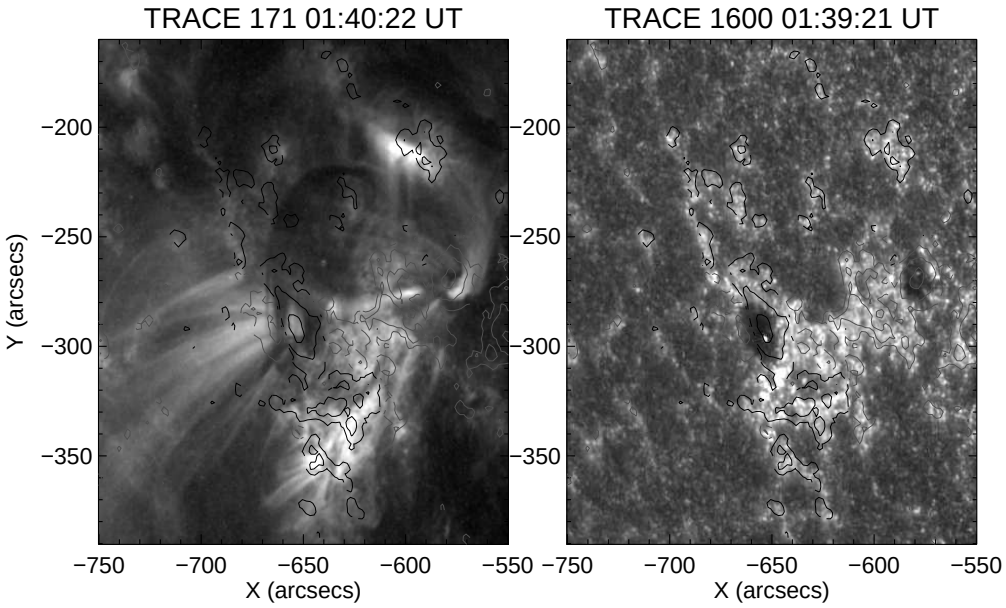

Fig. 1.— NOAA active region 10442 observed by *TRACE* prior to the whipping-like asymmetric filament eruption. The filament is observed as dark, loop-like features in TRACE 171 Å. The TRACE images are overlaid by a *SOHO* MDI magnetogram obatained at 01:39:02 UT on 2003 Aug 25. Contours levels are 50, 200 and 800 gauss for positive polarities (black), and -800, -200, and -50 gauss for negative polarities (grey).

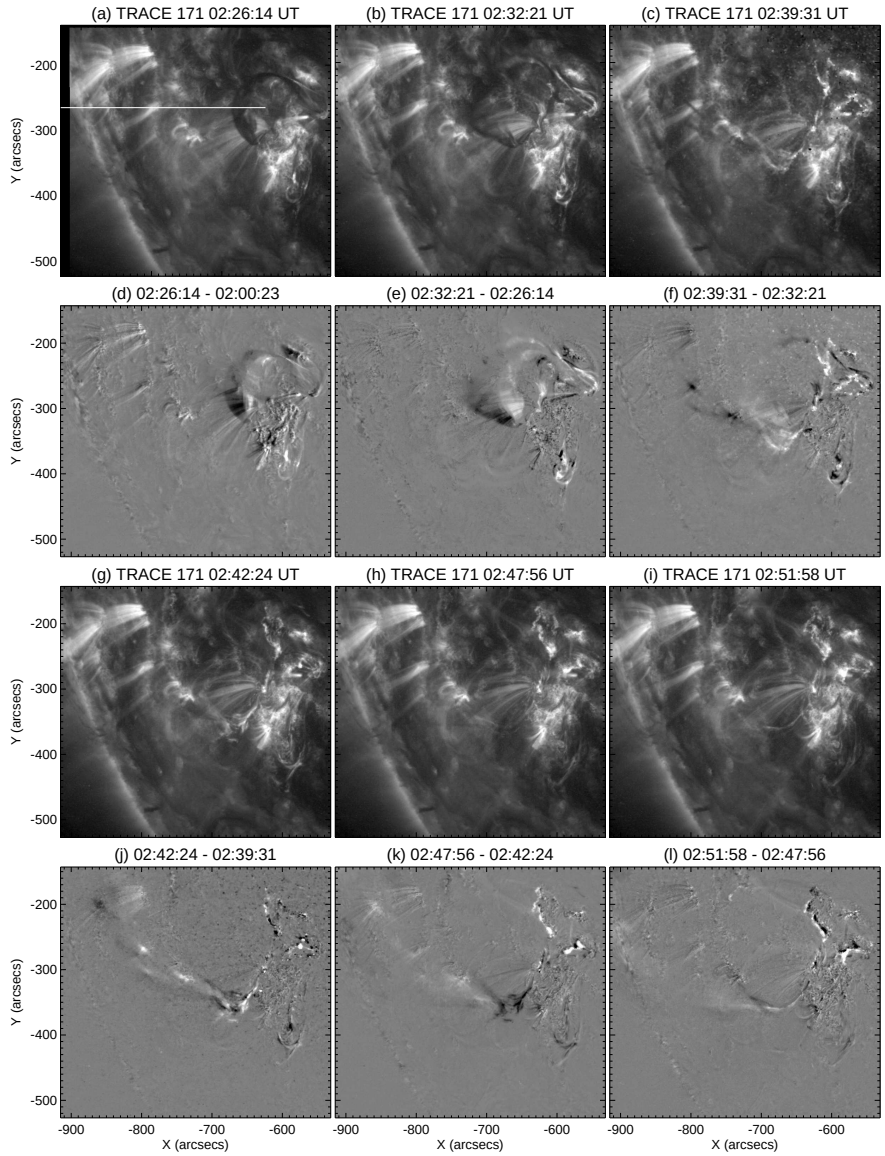

Fig. 2.— *TRACE* 171 Å and the corresponding running difference images showing a whipping-like asymmetric eruption. All images are co-registered with the *TRACE* 171 Å image taken at 02:00:23 UT. A fiducial is shown in (a) along which the projected displacements of the filament are measured (Fig. 4*a*). *TRACE* images with the same exposure duration, 55.1 s in this case, are used to conduct the running difference.

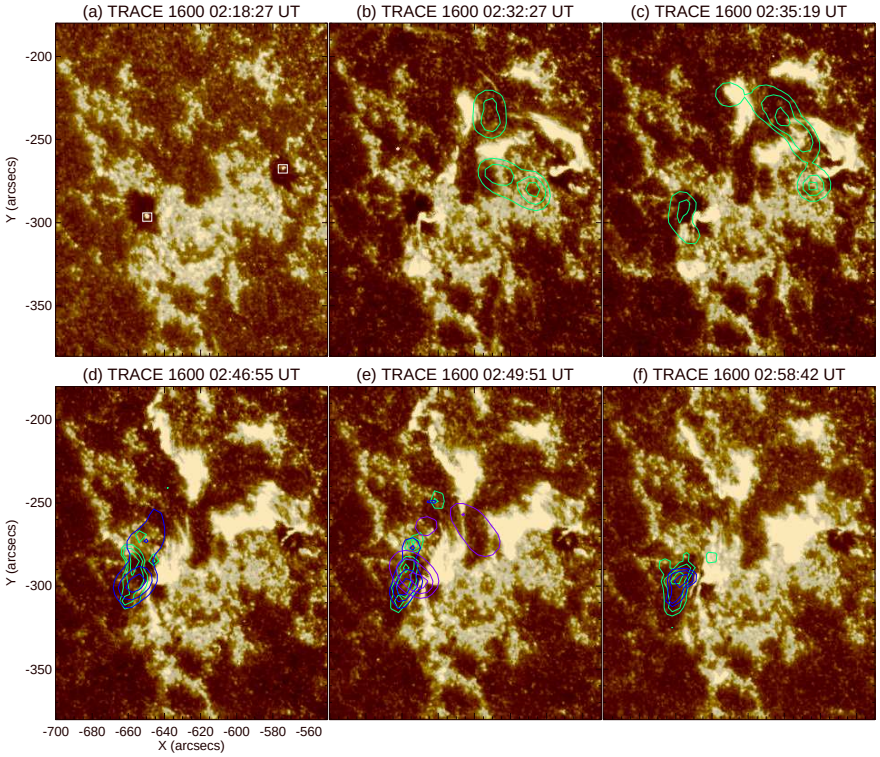

Fig. 3.— HXR source shifting observed in the 2003 August 25 event. The *TRACE* 1600 Å images are overlaid with *RHESSI* X-ray contours at 30%, 50% and 80% of the maximum intensity of each *RHESSI* image, in the 6–12 keV (green), 12–25 keV (blue), and 25–50 keV (purple) energy bands. The two boxes in (a) cover 11 by 11 pixels with the brightest pixel in the center, which enclose the two umbral brightenings. The evolution of the umbral brightenings with time are shown in Fig. 4*c*.

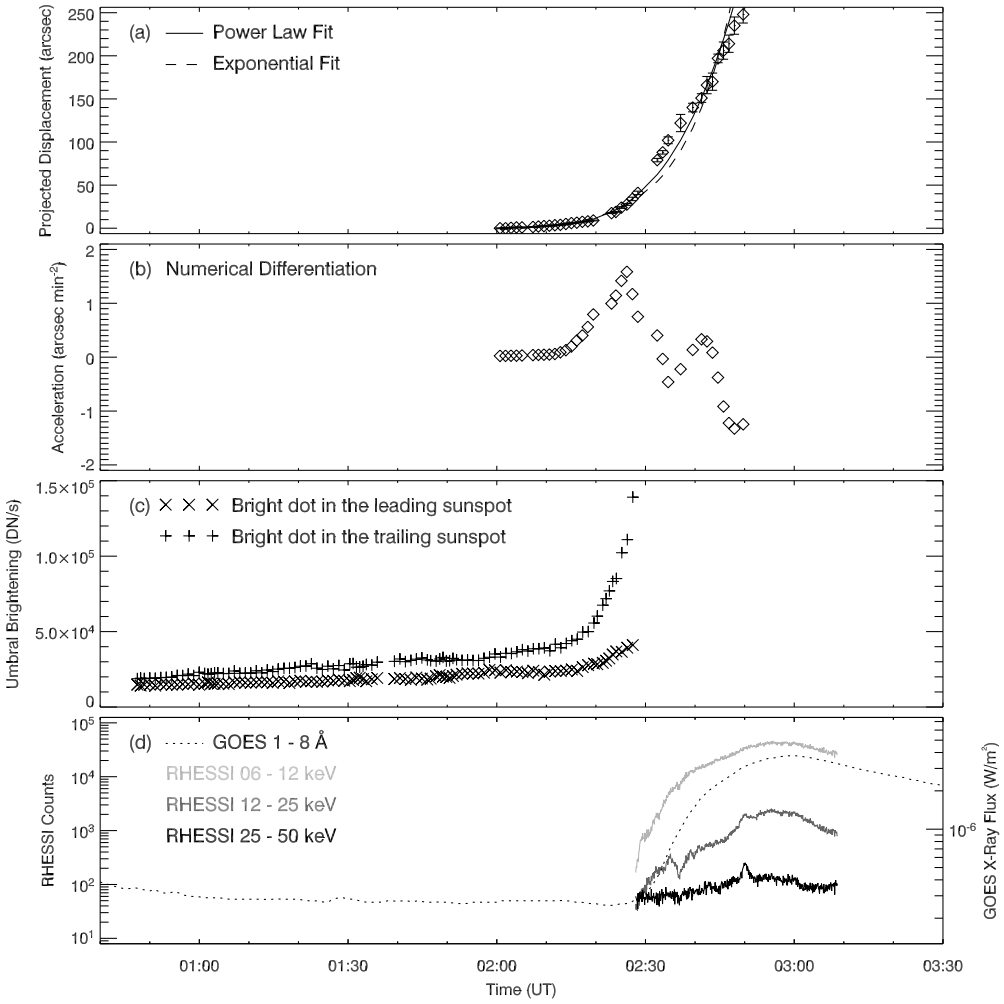

Fig. 4.— Dynamic evolution of the asymmetric eruptive filament on 2003 August 25 and the associated UV and X-ray emission. (*a*) Projected displacements of the filament in arcsecs, which are obtained by measuring the top of the filament along a fiducial as shown in Fig. 2*a*. The profile is fit with a power law function (solid line), $h = a + bt + ct^m$, and an exponential function (dashed line), $h = a + b\,exp(ct)$. (*b*) The acceleration of the filament (in arcsec min^{-2}, or 0.2 km s^{-2}, comparable to the Sun's surface gravity, 0.27 km s^{-2}) derived from (*a*). (*c*) The UV brightening in DN/s, which are obtained by integration over two boxes enclosing the bright dot in each sunspot, as shown in Fig. 3*a*. The measurement of the UV brightenings starts from 00:47:30 UT till 02:27:26 UT when the brightening in the trailing sunspot began to 'overflow' the defined box. (*d*) The y-axis on the left indicates accumulated photons recorded by *RHESSI* for every 4 s, in the 6–12 keV (light grey), 12–25 keV (grey) and 25–50 keV (black) energy bands. The 1-min average *GOES* flux (W m^{-2}) in the 1–8 Å band (dotted line) is scaled by the y-axis on the right.

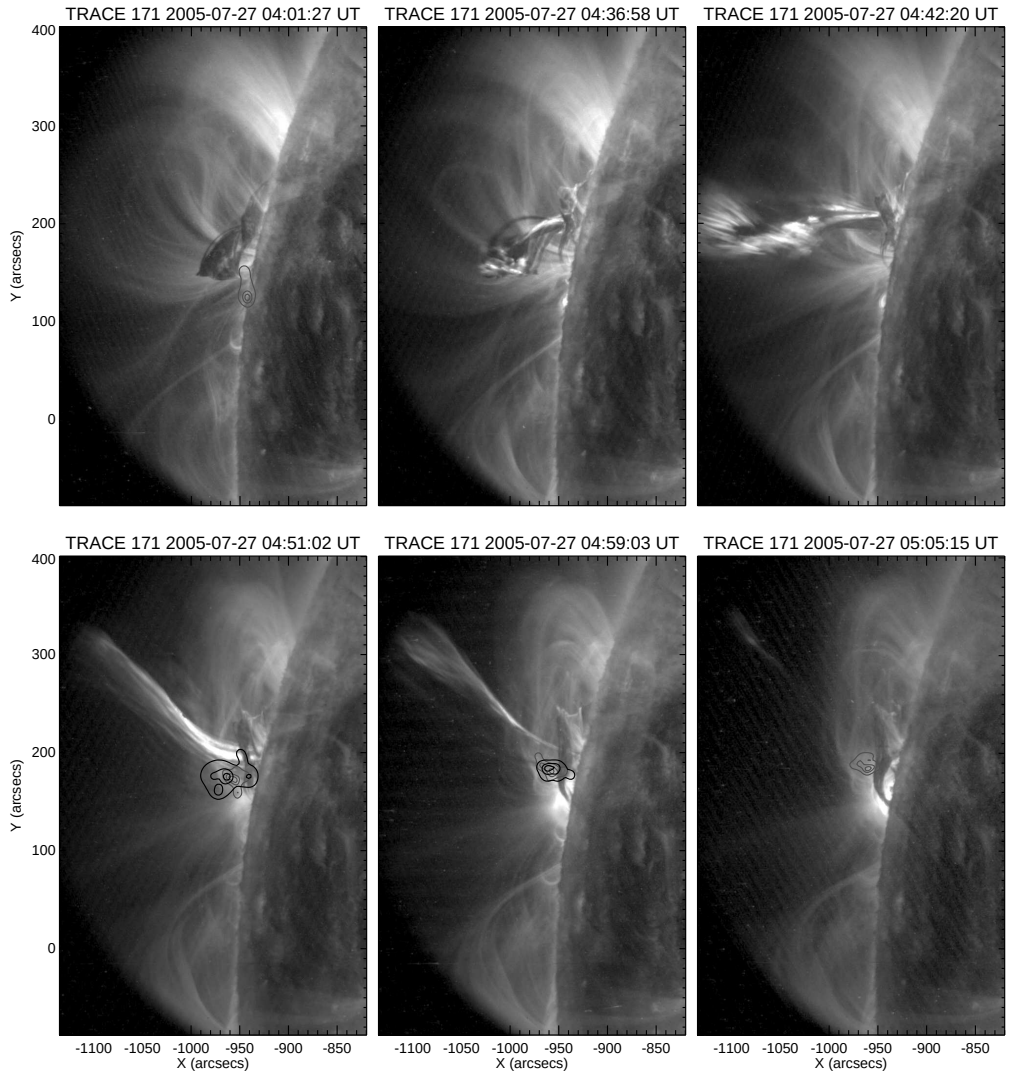

Fig. 5.— Whipping-like asymmetric filament eruption observed by *TRACE* on 2005 July 27. The *TRACE* 171 Å images are overlaid with *RHESSI* X-ray contours at 20%, 50% and 80% of the maximum intensity of individual *RHESSI* image, in 12–25 keV (grey), and 25–50 keV (black) energy ranges.

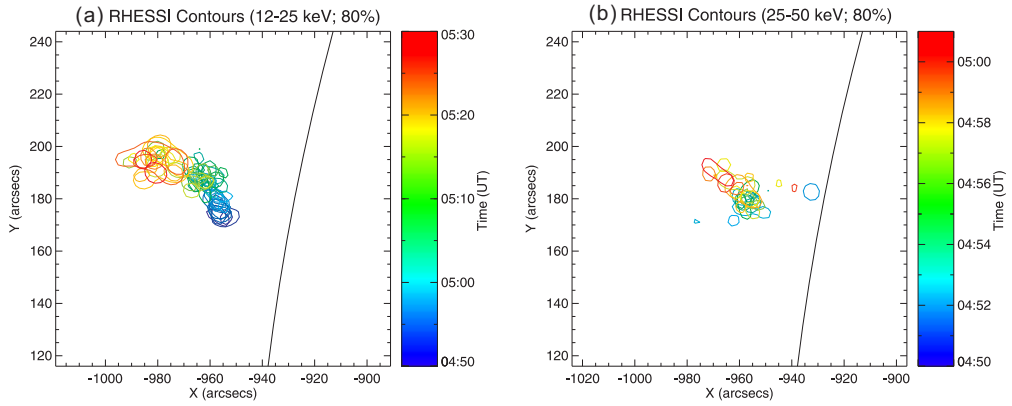

Fig. 6.— Hard X-ray coronal source shifting observed in the 2005 July 27 event. The contours represent the locations of the HXR source at 80% of the peak intensity at a specific time instant, coded by a color spectrum. (*a*) The HXR source in the 12–25 keV energy range. (*b*) The HXR source in the 25-50 keV energy range.

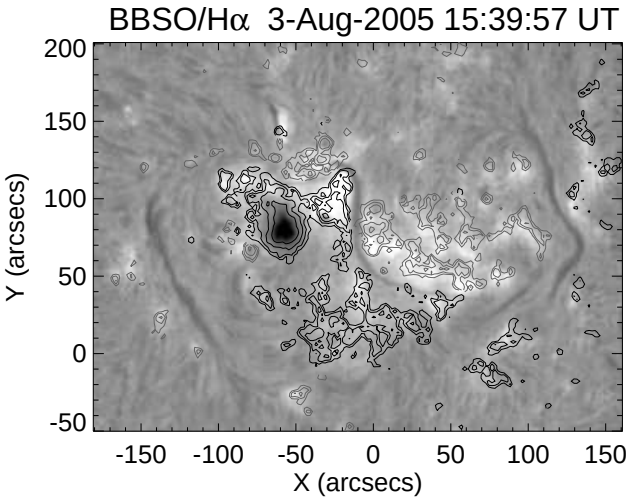

Fig. 7.— NOAA active region 10792 observed in Hα at the disk center on 2005 Aug 3 by Big Bear Solar Observatory. Overlaid black (grey) contours represent the magnitude of the line-of-sight photospheric magnetic field with positive (negative) polarities, observed by *SOHO* MDI.

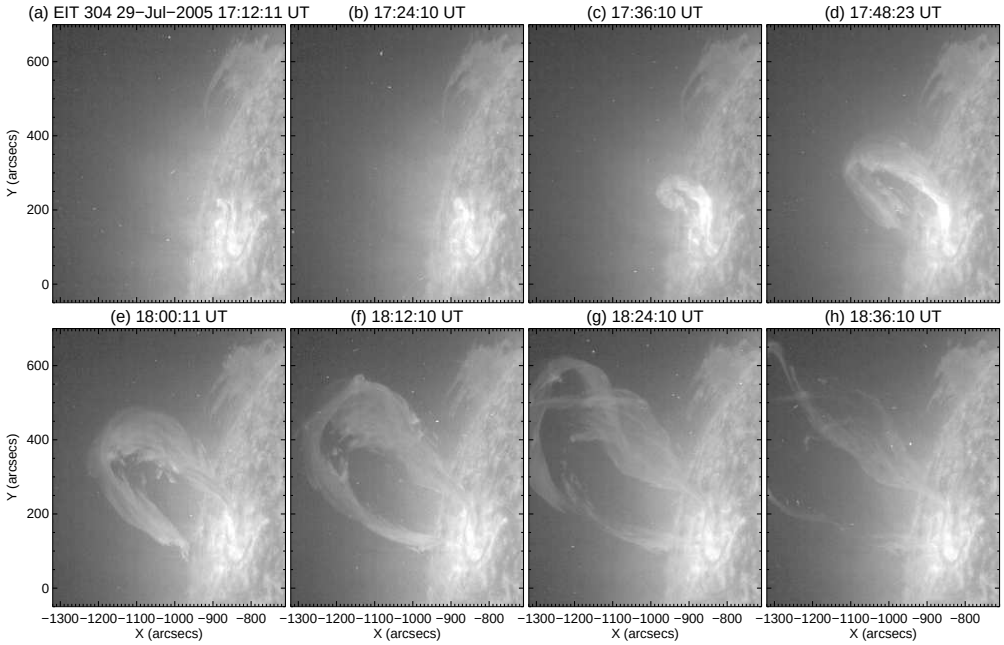

Fig. 8.— Zipping-like asymmetric filament eruption observed in *SOHO* EIT 304 Å filter on 2005 July 29.

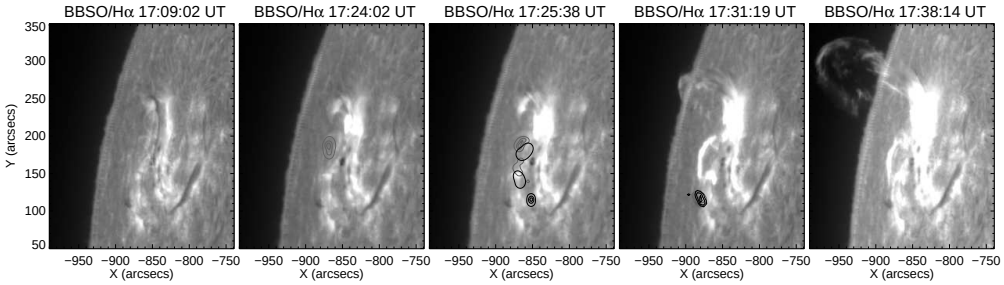

Fig. 9.— Shifting of the hard X-ray foot-point sources observed in the 2005 July 29 event. Hα images obtained at Big Bear Solar Observatory are overlaid with corresponding *RHESSI* contours at 20%, 50%, and 80% of the peak intensity of each *RHESSI* image in the 12-25 keV (grey) and 25-50 keV (black) energy ranges.

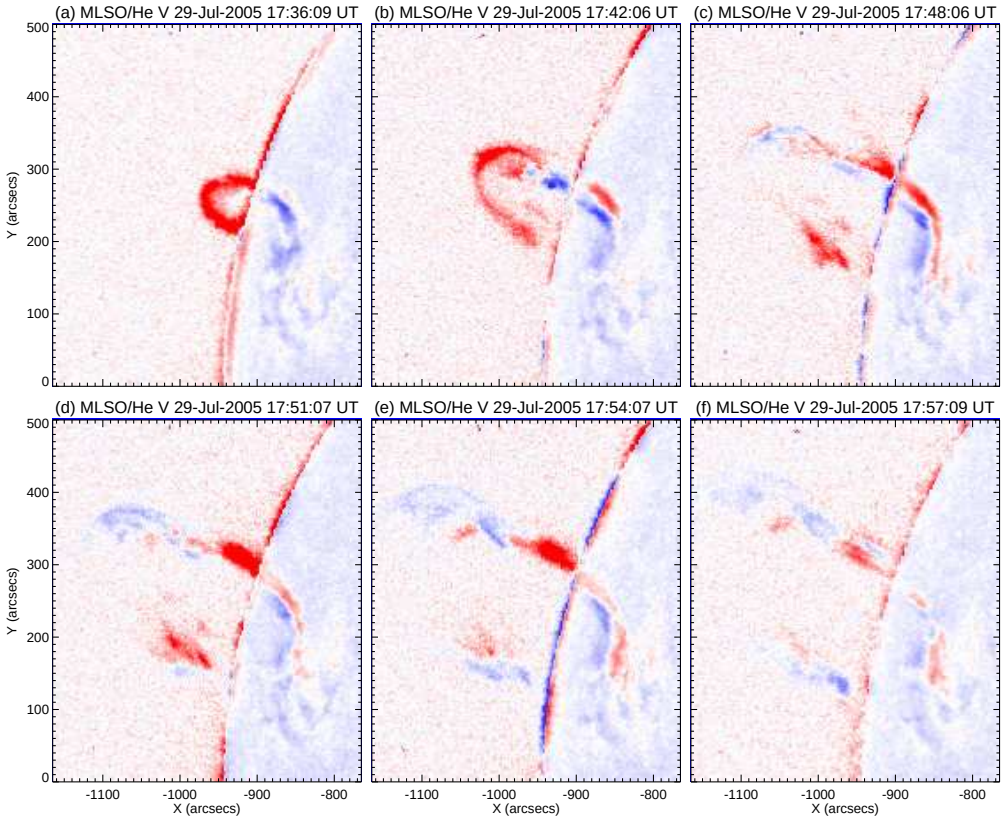

Fig. 10.— The zipping-like asymmetric filament eruption observed by the CHIP instrument operated at Mauna Loa Solar Observatory on 2005 July 29. Red (blue) colors indicate motions away (toward) the observer.

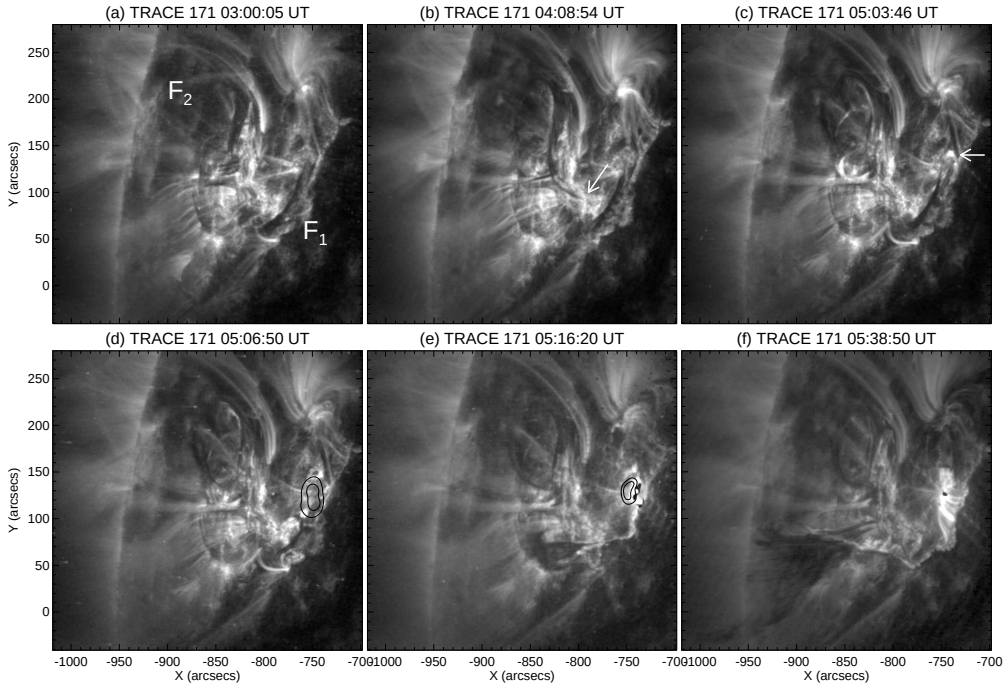

Fig. 11.— Activation and eruption of the whipping-like filament, "F_1", in the 2005 July 30 event. F_1 is located along the southern half of the S-shaped neutral line while the zipping-like filament, "F_2", which erupted later, is located along the northern half. *TRACE* 171 Å images are overlaid with *RHESSI* contours at 20%, 50%, and 80% of the peak intensity of each *RHESSI* image, in the 12-25 keV energy range.

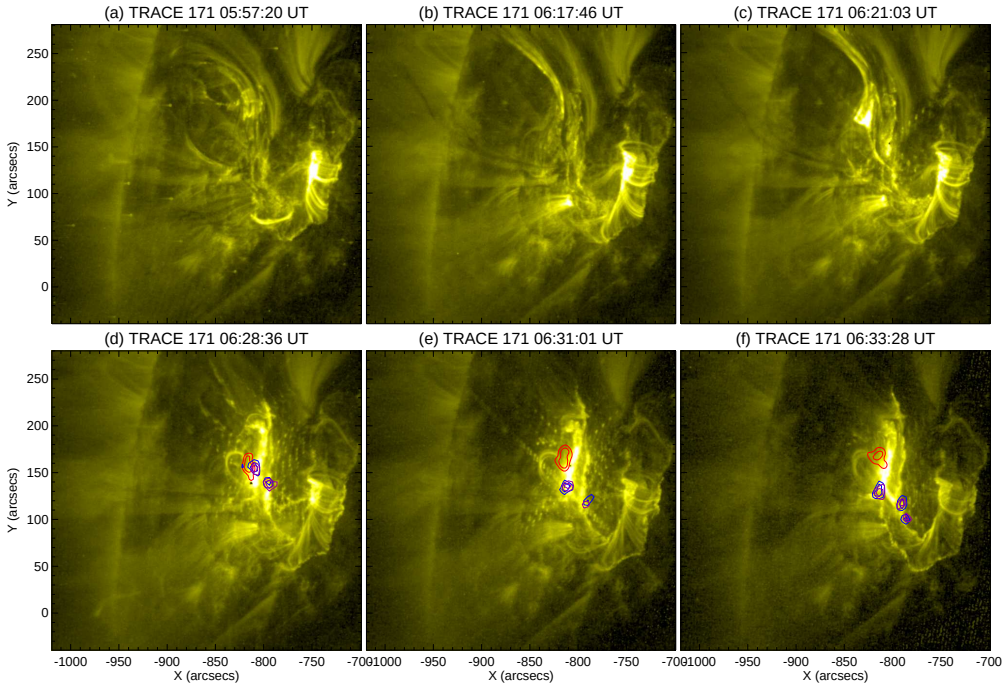

Fig. 12.— Eruption of the zipping-like filament, F_2, and the shifting of HXR footpoint sources observed in the 2005 July 30 event. *TRACE* 171 Å images are overlaid with *RHESSI* contours at 20%, 50%, and 80% of the peak intensity of each *RHESSI* image, in the 12–25 keV (red), 25–50 keV (blue) and 50–100 keV (purple) energy ranges. The shifting is observed from about 06:28 UT till 06:36 UT.

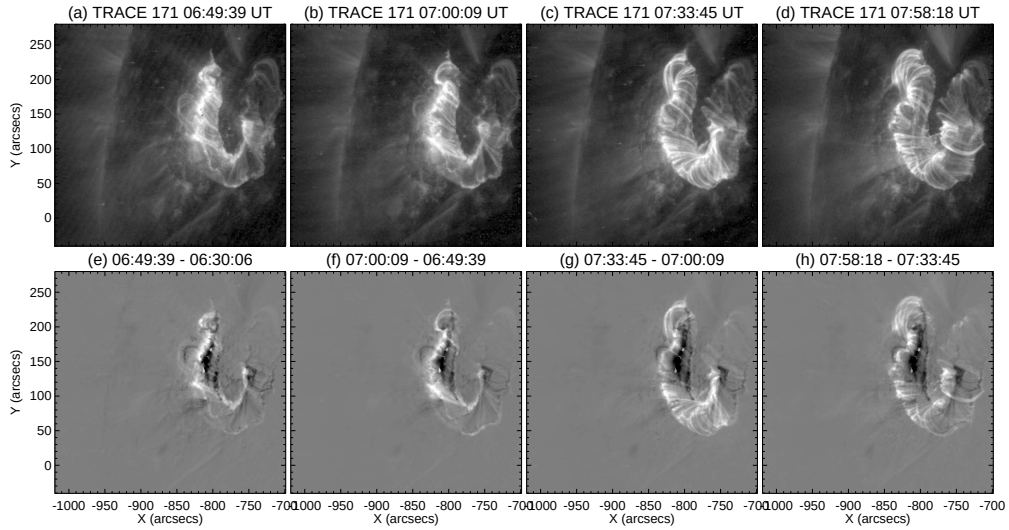

Fig. 13.— The propagation of the post-flare arcade brightening observed in the *TRACE* 171 Å filter on 2005 July 30. The bottom panel shows the corresponding base-difference images. Images with the same exposure time, 11.58 s in this case, are used in conducting the image difference.

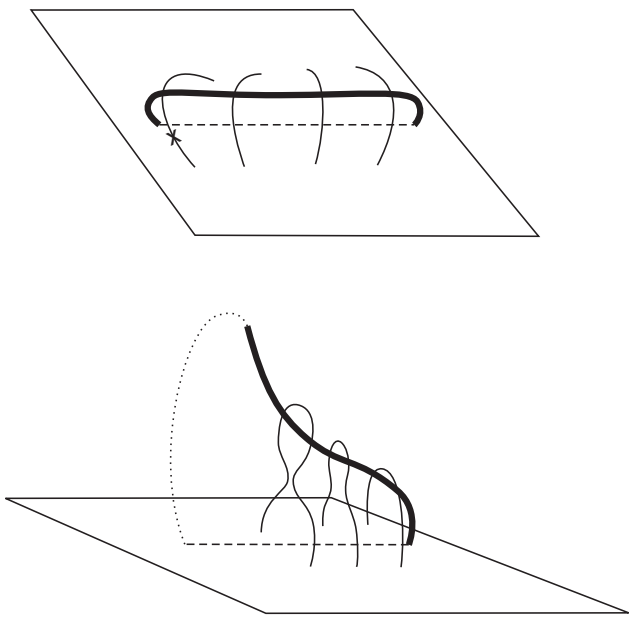

Fig. 14.— A cartoon showing a whipping-like asymmetric filament eruption. The filament is represented by a thick loop aligned along the magnetic neutral line, which is indicated by a dashed line. In the top panel the x mark indicates the tether release occurring at one end of the filament. As the filament whips upward, the magnetic field in the active leg may be still connected to the solar surface, as indicated by the dotted line.

Fig. 15.— Schematic diagrams for the two zipping-like eruptions: (*a*) the 2005 July 29 event, and (*b*), F_2 in the 2005 July 30 event. The thick loops in both panels indicate the filament, the dashed lines indicate the S-shaped neutral line, and the arrows indicate the direction in which the HXR sources shifted.

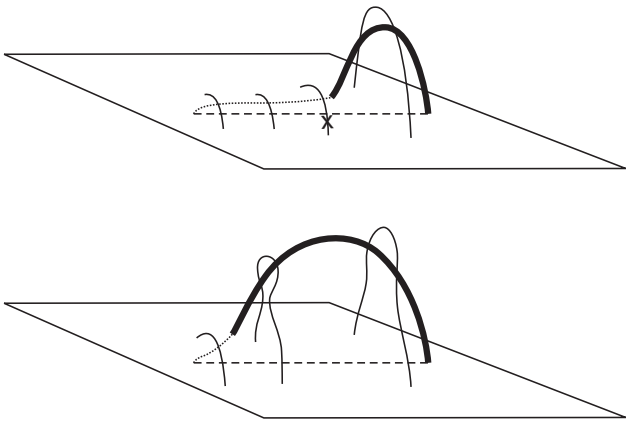

Fig. 16.— A cartoon showing a zipping-like asymmetric filament eruption. As in Fig. 14 and Fig. 15, the filament is represented by a thick loop, aligned along the neutral line which is indicated by a dashed line. In the top panel, the cross indicates that tether release occurs at the visible end of the active leg of the filament. In the bottom panel, the compact potential-like loops that originally overly the lower part of the active leg are stretched, and then reconnect beneath the filament.